

A SIMPLE LIKELIHOOD ESTIMATOR FOR QUASAR TARGET SELECTION

JESSICA A. KIRKPATRICK^{1,2}, DAVID J. SCHLEGEL², NICHOLAS P. ROSS², ADAM D. MYERS^{3,4,5}, JOSEPH F. HENNAWI³,
DONALD P. SCHNEIDER⁶, BENJAMIN A. WEAVER⁷

Submitted for publication in “The Astrophysical Journal”

ABSTRACT

We present a new method for quasar target selection using photometric fluxes and a likelihood estimator. For our purposes we target quasars using Sloan Digital Sky Survey (SDSS) photometry to a magnitude limit of $g = 22$. The efficiency and completeness of this technique is measured using the Baryon Oscillation Spectroscopic Survey (BOSS) Data, taken in 2010. This technique was used as the CORE method for target selection for BOSS Year One spectroscopy to be realized in the 9th SDSS data release. When targeting at a density of 40 objects per sq-deg (the BOSS quasar targeting density) the efficiency of this technique in recovering $z > 2.2$ quasars is 40%. The completeness compared to all quasars identified in BOSS Data is 65%. This paper also describes possible extensions and improvements for this technique.

Subject headings: cosmology: observations, large-scale structure of universe, quasars: general, surveys

1. INTRODUCTION

Quasars (QSOs) have been vital astrophysical tools since their discovery over forty years ago (Matthews & Sandage 1963; Schmidt 1963). Individually, quasars provide examples of energetic and extreme physics, e.g., the broad absorption line phenomenon, first characterized by Bahcall & Goldsmith (1971); Weymann et al. (1981, 1991), and more recently by e.g., Gibson et al. (2009); Allen et al. (2011). Quasars are also tracers of structure at large scales (e.g., Croom et al. 2005; Myers et al. 2006, 2007a,b; Shen et al. 2007, 2009; Ross et al. 2009) and small scales (Hennawi et al. 2006a; Myers et al. 2007b; Myers et al. 2008), providing constraints on their host dark matter halos and the quasar phenomenon (Shankar 2009; Shen 2009). Due to their intrinsic luminosity (\sim few 10^{46} erg s^{-1}) they can be seen to high ($z \sim 6$) redshifts (e.g., Fan et al. 2006b; Willott et al. 2010), enabling constraints to be placed on the epoch of reionization (EoR; Fan et al. 2006a). Furthermore, there is now strong evidence that there is a link between luminous AGN activity and the formation and evolution of massive galaxies (see Cattaneo et al. 2009 for a review).

Quasars have proved to be cosmological “backlights” and the absorption features blueward of the Lyman- α (1216Å) emission line have been seen in tradition-

ally bright quasar spectra (Rauch 1998 and references therein). The absorption between the Lyman- α and the Lyman-limit (912 Å), caused by neutral hydrogen, is referred to as the Lyman- α forest (Ly α F; Lynds 1971). The region between Lyman- α and Lyman- β is typically used for Ly α F science because it is not confused by Lyman- β absorption lines. Meiksin (2009) has a contemporary review, with the importance of the Ly α F in cosmology discussed by Croft et al. (1998) and White (2003), and measured, via the (“1-D”) Power Spectrum, by Croft et al. (2002) and McDonald et al. (2006).

The Ly α -forest begins to appear in the near-UV/blue bands at $z \sim 2$. If Ly α F lines of sight are observed at high spatial density, then they can be used to perform precise measurements of the expansion rate and distance scale and thus constrain cosmological world models (White 2003; McDonald 2003; McDonald & Eisenstein 2007; McQuinn & White 2011).

Previous quasar surveys, such as the Sloan Digital Sky Survey (SDSS; Schneider et al. 2010) and the Anglo-Australian Telescope Two-Degree Field (2dF) QSO Redshift Survey (2QZ; Croom et al. 2004), have historically performed quasar target selection by searching for relatively bright quasars ($i < 19.1$, $z < 3$ objects for SDSS). However, previous methods, such as the traditional UV Excess (UVX; selecting star-like objects with unusually blue broadband colors, Sandage (1965)) or color-boxes (Richards et al. 2006; Croom et al. 2009) begin to fail at fainter magnitudes because since photometric errors will broaden the stellar locus, leading to potential incompleteness and inefficiency in target selection. This motivated our development of a selection technique which better handles the photometric flux errors as one approaches the flux limit.

Furthermore, at $z > 2$ broad-band optical color selections fail, since the colors of these quasars are similar to those of stars (in particular early A and F stars, Fan

¹ Department of Physics, The University of California, Berkeley, CA 94720, USA; kirkpatrick@berkeley.edu

² Lawrence Berkeley National Laboratory, 1 Cyclotron Rd, Berkeley, CA 92420, USA

³ Max-Planck-Institut für Astronomie, Knigstuhl 17, 69117 Heidelberg, Germany

⁴ University of Illinois, 1002 West Green Street, Urbana, IL 61801, USA

⁵ Department of Physics & Astronomy, University of Wyoming, Laramie, WY 82071, USA

⁶ Department of Astronomy & Astrophysics, The Pennsylvania State University, University Park, PA 16802, USA

⁷ Center for Cosmology and Particle Physics, New York University, New York, NY 10003 USA

1999, Richards et al. 2002) as the quasars “pass over the stellar locus” when the photometric fluxes are the same as the stellar fluxes (see Section (3.2) for more details). Simultaneously, quasars become much fainter e.g., an $M_g = -23$ quasar at $z = 2$, has g -band ~ 21.7 , which is close to the SDSS single-epoch magnitude limit.

With the final data release of the SDSS (Abazajian et al. 2009), an incredibly powerful database of over 100,000 spectroscopically confirmed quasars (Schneider et al. 2010) and 1,000,000 photometric potential quasar targets (Richards et al. 2009) is now publicly available. In particular, the Richards et al. (2009) photometric sample is the largest sample of photometrically classified $z > 2.4$ quasars in the literature. This catalog has been the dataset of several cosmology studies including: studies of cosmic magnification bias (Scranton et al. 2005); the investigation into the clustering of quasars on large (Myers et al. 2006, 2007a) and small (Hennawi et al. 2006a; Myers et al. 2007b; Myers et al. 2008) scales; the Integrated Sachs-Wolfe (ISW) effect (Giannantonio et al. 2006; Giannantonio et al. 2008); binary quasars (Hennawi et al. 2006b, 2010b; Prochaska & Hennawi 2009; Shen et al. 2010); and the near infrared photometric properties of quasars (Peth et al. 2011).

The SDSS-III: Baryon Oscillation Spectroscopic Survey (BOSS; Eisenstein et al. 2011) is specifically targeting $z > 2.2$ QSOs in order to observe 150,000 Ly α F lines of sight. The key aim of BOSS is to measure the absolute cosmic distance scale and expansion rate with percent-level precision at three distinct cosmological epochs: redshifts $z = 0.3, 0.6$ using luminous red galaxies (LRGs) and $z \sim 2.5$ using the Ly α F, via the baryon acoustic oscillation (BAO) technique (Schlegel et al. 2007, 2009; Slosar et al. 2011). BOSS plans to dedicate 40 fibers deg^{-2} to QSO target selection for measuring the BAO signal.

The BOSS Ly α F/Quasar Survey will target objects thought to be $z > 2.2$ quasars to perform a Ly α F BAO measurement. Since the foreground Ly α F is independent of the intrinsic properties of the background quasar, there is freedom to use multiple selection methods without biasing the BAO results. The methods used for BOSS targeting include the “Kernel Density Estimator” (KDE; Richards et al. 2004), an “Extreme-Deconvolution” method (XDQSO; Bovy et al. 2011), and a Neural Network method (NN; Yèche et al. 2010). The BOSS QSO target selection used for the first year of observations (Ross et al. 2011) combines all these different methods, including the Likelihood method described in this paper, with different photometric catalogs such as SDSS (York et al. 2000), UKIDSS (Lawrence et al. 2007), GALEX (Martin et al. 2005) and quasars found using their flux time-variability information (Palanque-DeLabrouille et al. 2010).

BOSS uses the same imaging data as that of the original SDSS-I/II survey, with an extension in the South Galactic Cap (SGC) (York et al. 2000). These data were gathered using a dedicated 2.5 m wide-field telescope (Gunn et al. 2006) to collect light for a camera with 30 2k \times 2k CCDs (Gunn et al. 1998) over five broad bands - *ugriz* (Fukugita et al. 1996); this camera has imaged 14,555 unique deg^2 of the sky, including 7,500 deg^2 in the North Galactic Cap (NGC) and 3,100 deg^2 in the SGC

(SDSS-III collaboration et al. 2011). The imaging data were taken on dark photometric nights of good seeing (Hogg et al. 2001), and objects were detected and their properties were measured (Lupton et al. 2001; Stoughton et al. 2002) and calibrated photometrically (Smith et al. 2002; Ivezić et al. 2004; Tucker et al. 2006; Padmanabhan et al. 2008), and astrometrically (Pier et al. 2003).

Padmanabhan et al. (2008) present an algorithm which uses overlaps between SDSS imaging scans to photometrically calibrate the SDSS imaging data. BOSS target selection uses these “ubercalibrated” data from the SDSS Data Release Eight (DR8) database (SDSS-III collaboration et al. 2011). The 2.5° stripe along the celestial equator in the Southern Galactic Cap, commonly referred to as “Stripe 82” was imaged multiple times, for up to 80 epochs spanning a 10-year baseline (Abazajian et al. 2009). A coaddition of these data (Adelman-McCarthy et al. 2008) goes roughly two magnitudes fainter than the single-scan images which make up the bulk of the SDSS imaging data.

In this paper we describe a new method for quasar target selection. Our method models data in 5-filter flux space, then calculates likelihood estimates that a given object is a high- z (> 2.2) quasar. Because a given survey has a finite number of spectroscopic fibers (observing time allocation) to dedicate towards quasar targeting, this method attempts to prioritize selection by calculating a probability that a potential target is a quasar based on these likelihood calculations. Targets are ranked by likelihood probability. This method differs from KDE in that it incorporates the photometric errors into the likelihood calculations; also KDE only imposes a single magnitude prior and color-distribution, whereas we model the QSO density as a function of magnitude and evolution of color distribution.

The layout of this paper is as follows. Section (2) describes the method used to calculate the likelihoods, and training catalogs that are generated and used for Likelihood target selection. In Section (3) we give an overview of the BOSS Data and the performance of the Likelihood method using this data. In Section (4) we discuss testing and optimization of the method, as well as future work and possible improvements. We use the terms “quasar” and “QSO” interchangeably to refer to quasi-stellar, type-I broad line objects. All Right Ascension (RA) and Declinations (Dec) discussed are J2000.

Our Likelihood method was the “CORE” method used in the first year of the BOSS QSO target selection (Ross et al. 2011) and it is our intention to release our calculated likelihood probabilities as a data product in the future Data Releases of the BOSS (the first such event is SDSS Data Release 9).

2. METHOD AND CATALOG GENERATION

2.1. Likelihood Estimator

A straightforward approach to spectroscopic quasar target selection is an object-by-object probability estimation from large training sets. A potential target is assigned a probability that it is a quasar by comparing the fluxes of the target to fluxes of all the objects in the training sets. This is done by calculating a likelihood using a catalog of known quasars (QSO) and comparing this to a likelihood using a catalog of all other non-

quasar observable objects (stars + galaxies + anything else), hereafter referred to as Everything Else (EE).

These likelihoods[†] are defined as follows:

$$\mathcal{L}_{QSO}(\Delta z) = \sum_i \prod_f \sqrt{\frac{1}{2\pi\sigma_f^2}} \exp\left(-\frac{[x_f - QSO_{if}(\Delta z)]^2}{2\sigma_f^2}\right) \quad (1)$$

Note that \mathcal{L}_{QSO} is separated into redshift bins (Δz) so that we can tune this likelihood to a desired QSO target redshift range.

$$\mathcal{L}_{EE} = \sum_i \prod_f \sqrt{\frac{1}{2\pi\sigma_f^2}} \exp\left(-\frac{[x_f - EE_{if}]^2}{2\sigma_f^2}\right) \quad (2)$$

where x_f is the flux and σ_f is the error in flux in filter f of any single potential target (O); QSO_{if} is the flux of a single object (i) in the QSO catalog; EE_{if} is the flux of a single object (i) in the Everything Else catalog; the f products are over the five SDSS filters; and the i summations are over all objects in the respective training catalogs. We used SDSS photometric PSF fluxes (x_f) from the SkyServer (<http://www.sdss3.org/dr8/>) under the standard SDSS data releases.

All fluxes and their errors are corrected for Galactic extinction in the SDSS filters using the prescription in Schlegel et al. (1998). Because the sum is done in flux space rather than color space, object errors are independent. Also, our method preserves the luminosity function information, whereas the absolute flux information is lost when using colors. Our catalogs use stacked (co-added) fluxes (see Section (2.2) and Section (2.3)), whereas the targets are single epoch fluxes (see Section (3.2)). Therefore in the above equations, the errors in the catalog fluxes (QSO_{if} and EE_{if}) are ignored because the signal-to-noise ratio of the catalog fluxes are much greater than the signal-to-noise ratio of our potential targets (x_f). The QSO likelihoods are calculated as a function of redshift (Δz) by subdividing the objects in the QSO catalog data into redshift bins of width $\Delta z = 0.1$ (e.g. $0.5 \rightarrow 0.6$, $0.6 \rightarrow 0.7 \dots 4.9 \rightarrow 5.0$). The Gaussian normalizations add a multiplicative constant to each likelihood (\mathcal{L}), which is the same for both Eq. (1) and Eq. (2) for a given target and cancel when calculating the probabilities described below.

The probability that a single potential target object (O) is a quasar (QSO) in a target redshift range is defined by the following conditional probability where the numerator is the likelihood of the target being a QSO in the desired redshift range and the denominator is the likelihood of it existing in the entire catalog space:

$$\mathcal{P}(O \in QSO) = \frac{\sum_{z_{\text{target}}} \left(\frac{\mathcal{L}_{QSO}(z)}{A_{QSO}}\right)}{\frac{\mathcal{L}_{EE}}{A_{EE}} + \sum_{z_{\text{all}}} \left(\frac{\mathcal{L}_{QSO}(z)}{A_{QSO}}\right)} \quad (3)$$

The normalization factors A_{QSO} and A_{EE} are the sky area of the QSO and EE catalogs respectively, and thus each summation is a relative density, and Eq. (3) is a true conditional probability ($\mathcal{P} \in [0, 1]$) using Bayes' theorem.

[†] We use the term ‘‘likelihood’’ to denote a conditional probability that our target object (O) with fluxes (x_f) belongs to the class A ($QSO(\Delta z)$, EE); $p(\{x_f\} | O \in A)$

In the numerator, $\mathcal{L}_{QSO}(z)$ is summed over the desired quasar target redshift range (z_{target}), whereas the denominator contains all objects in both catalogs summed over the entire redshift range (z_{all}). These probabilities are exact in the limit of perfect training catalogs (infinite objects and zero errors). A probability is calculated for every potential target using the full catalogs.

2.2. QSO Catalog

Because there are relatively few previously observed quasars in the desired BOSS redshift range ($z > 2.2$) with sufficiently low flux errors to precisely describe the quasar color locus, for our purposes the QSO Catalog is generated by a Monte Carlo technique (Hennawi et al. 2010a) to provide a less biased and more complete sample than is available from the SDSS quasar catalog. The Monte Carlo simulation uses a model of the quasar luminosity function based on the studies by Jiang et al. (2006) to compute the density of quasars as a function of redshift and i -magnitude. The Jiang et al. (2006) luminosity function is used because it reaches fainter than the luminosity function of Richards et al. (2006) and thus better matches the high redshift quasars in the BOSS redshift regime. SDSS Data Release 5 spectroscopically confirmed quasars (DR5QSO; Schneider et al. 2007) are the photometric inputs to the Monte Carlo. The simulation generates 9.94 million unique (i -magnitude, redshift) pairs down to $i = 22.5$ (0.5-mag fainter than the BOSS magnitude limit) with a distribution given by the luminosity function. Each simulated quasar (QSO_i) is then matched to the SDSS quasar (DR5QSO) with the nearest redshift to QSO_i . The SDSS photometry of the DR5QSO quasar is rescaled such that its i -magnitude matches that of the simulated quasar (QSO_i). We assume that quasar colors are not a function of magnitude in the redshift range of interest, and thus can be extrapolated in this manner to deeper fluxes. Thus this technique preserves the relative fluxes while providing a more complete coverage of the flux space than only using known SDSS quasars. Finally, only objects with redshifts in the range desired for BOSS targeting ($z > 2.2$)

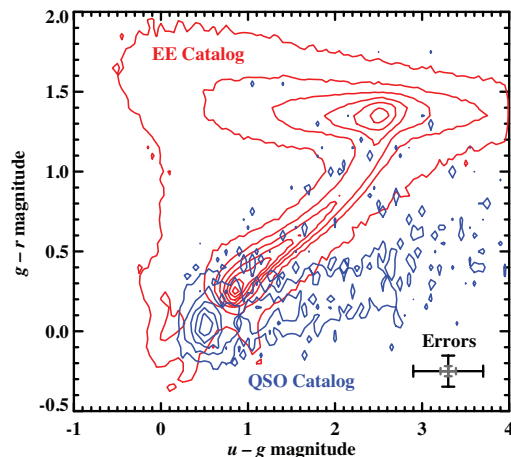


FIG. 1.— Contour plot of the $u-g$ and $g-r$ colors of the Everything Else (red) and QSO (blue) Catalogs. The region of overlap, where target selection becomes difficult, is at $u-g \approx 1$ and $g-r \approx 0$. The error bars are the SDSS single-epoch $g-r$ and $u-g$ magnitude errors at $g=22$ (black) and $g=20$ (grey).

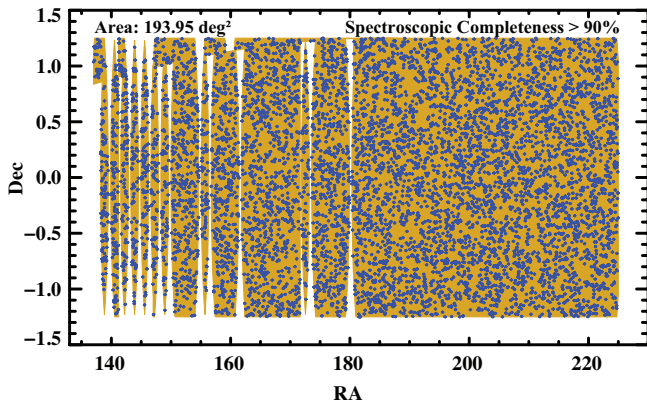


FIG. 2.— Right Ascension (RA) versus Declination (Dec) of BOSS QSO Data used for the Likelihood method testing and luminosity function testing. Testing was done in the Stripe 82 calibration band with regions of high ($> 90\%$) spectroscopic completeness. The blue points are spectroscopically confirmed quasars and the yellow regions are the sky tiles that were observed. Note that the vertical and horizontal scales are not the same.

are included in the numerator of Eq. (3). The location in ugr color-color space of the $z > 2.2$ objects in the QSO Catalog is shown by the blue contours in Fig. (1).

2.3. Everything Else Catalog

The Everything Else (EE) Catalog is generated using stacked SDSS “Stripe 82” imaging, allowing the construction of a large point source catalog with variability information and smaller errors than possible using single-epoch SDSS imaging. Stripe 82 is the 2.5° wide region on the celestial equator between $RA = -45^\circ$ and $RA = 45^\circ$ where SDSS repeatedly scanned. Non-photometric data were ignored, and the photometric images were processed with a version of the SDSS photometric reduction pipeline similar to that in Data Release 8 (SDSS-III collaboration et al. 2011). The photometric depth is $r \sim 22.5$ magnitude (5σ) for point sources, with high completeness and accurate star-galaxy separation to $r \sim 22$ magnitude. These data were combined at the catalog level to produce co-added PSF photometry. Typically 20 observations were included for each object, resulting in a co-added catalog with typical errors of 6.1%, 2.4%, 3.0%, 7.1% and 27% at 22nd magnitude in the u, g, r, i, z filters, respectively.

The EE Catalog is further trimmed to a clean sample of non-variable point sources for inclusion in the likelihood calculations of Eq. (3). The 23.9% of objects that are blended with neighboring objects are rejected, thus reducing the effective footprint of this catalog from 225 deg^2 to 171.2 deg^2 . Objects with high variability are explicitly excluded from the catalog under the presumption that these are dominated by quasars (Schmidt et al. 2010), and we explicitly add quasars into the numerator and denominator of Eq. (3) such that the computed probability remains in the range $[0,1]$. These variable objects are identified as those with a reduced χ^2 of the fit to a constant r -band flux exceeding 1.4. This reduces the catalog to an effective area of 150 deg^2 . The result is a catalog with 1,042,262 photometric fluxes that represent all non-quasar types of objects. We determined the contamination of $z > 2.2$ quasars in this set is less than 0.5% by comparing this catalog with those for which we

have spectra. In Fig. (1) the red contours show the ugr color-color space of the objects in the EE catalog.

3. BOSS DATA & LIKELIHOOD PERFORMANCE

3.1. BOSS Stripe 82 Data

In September of 2009, BOSS started taking spectroscopic data. During the first year of data taking, several target selection methods were employed. In addition to Likelihood method, three other selection techniques were deployed: the KDE method developed to classify quasars by separating them from stars in color space (Richards et al. 2004), an “Extreme-Deconvolution” method (Bovy et al. (2011), Section (4.3)) and a new approach based on Artificial Neural Networks (Yèche et al. 2009). Previously spectroscopically confirmed quasars, as well as objects with high variability (Palanque-Delabrouille et al. 2010) over consecutive Stripe 82 runs were also targeted during this time.

Stripe 82 target selection used co-added catalog data from SDSS as the potential target fluxes. Because the co-added photometry has a higher signal-to-noise ratio than any single-epoch data run and the target fiber density in this region was higher than the rest of the survey, BOSS QSO completeness is highest in this region. Once observed, all of the quasar targets were automatically classified and then visually examined.

Based on the objects selected in Stripe 82, we found that the performances of the four methods were not identical as a function of the magnitude and redshift of the objects (Ross et al. 2011). This behavior is likely due to the different strategies adopted in the training of the methods.

3.2. Likelihood Performance

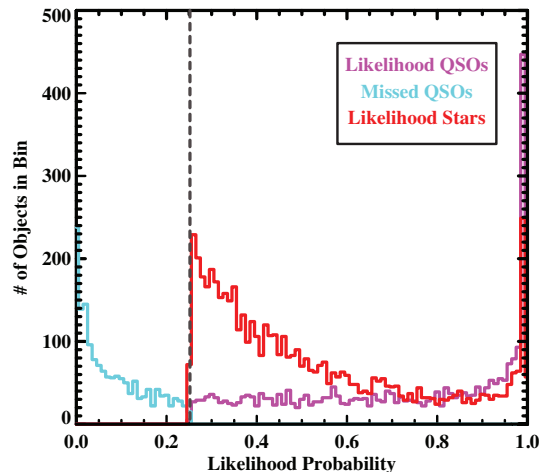


FIG. 3.— The likelihood probability (\mathcal{P}) distributions of the Likelihood method recovered QSOs (magenta, 4617 total), false-negative QSOs that were missed by the Likelihood method (cyan, 1566 total), and false-positive stars that were incorrectly targeted by Likelihood method (red, 5743 total). The vertical gray dashed line shows the likelihood \mathcal{P} threshold used for targeting ($\mathcal{P} > 0.245$). The spike around $\mathcal{P} = 0$ in the cyan curve are quasars that fall in the midst of the stellar locus and therefore are found by the method to have a very low probability of being QSOs. Most of these quasars are targeted because they are previously spectroscopically confirm QSOs or by their flux variability. The likelihood distribution of the probabilities for the not targeted stars (true-negative) are not included in the plot, but constitute an additional 742,662 objects.

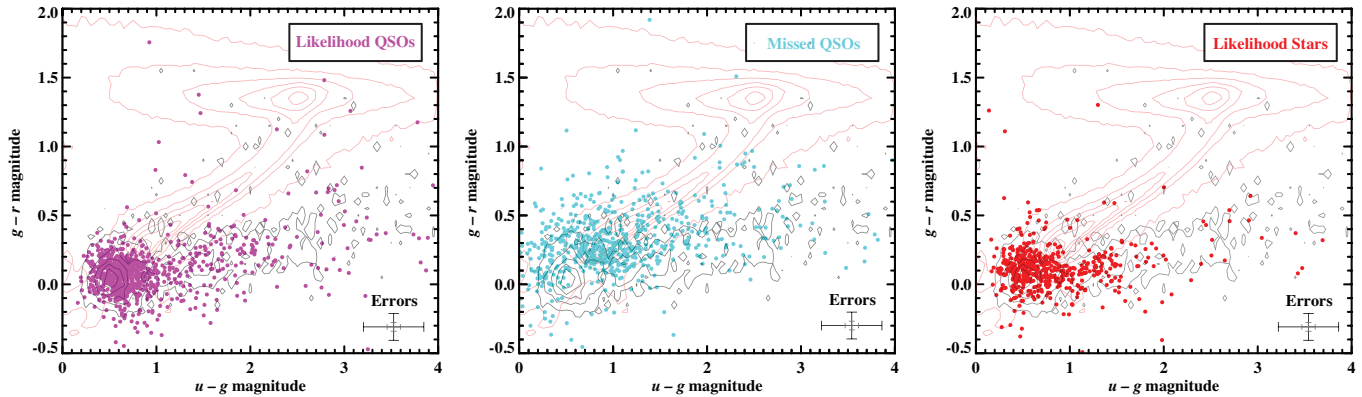


FIG. 4.— Color-color diagrams of BOSS QSOs recovered by the Likelihood method (*magenta*), false-negative QSOs that were not targeted (missed) by Likelihood method (*cyan*), and false-positive stars that were wrongly targeted by Likelihood method (*red*). These plots show recovered/missed ($z > 2.2$) QSOs. It is clear when comparing these plots with Fig. (1) that the problematic region for Likelihood targeting is where the two catalogs overlap near $u - g = 1$, $g - r = 0.25$. For context the QSO Catalog and EE Catalog contours plot from Fig. (1) are included in the above plots. The error bars are the SDSS single-epoch $g - r$ and $u - g$ magnitude errors at $g = 22$ (*black*) and $g = 20$ (*grey*). The targeting decisions were computed in flux space rather than the color space shown in the figures.

TABLE 1
LIKELIHOOD STRIPE 82 RESULTS
JIANG ET AL. (2006) LUMINOSITY FUNCTION

Targets per deg ²	Likelihood \mathcal{P} Threshold	Total Targets	QSOs Recovered	QSOs Missed	Completeness (%)	Efficiency (%)
5	0.974	969	669	3811	15	69
10	0.833	1938	1276	3227	28	66
20	0.535	3878	2166	2401	47	56
40	0.245	7757	3087	1657	65	40
60	0.136	11636	3595	1331	73	31
80	0.088	15515	3965	1108	78	26
100	0.063	19394	4219	980	81	22
140	0.037	27152	4618	806	85	17

NOTE. — The completeness and efficiency as a function of dedicated target fibers (targets deg⁻²). These values are for $z > 2.2$ recovered/missed QSOs. There is a trade-off: the more fibers given to targets, the more QSOs are found (greater completeness), but the accuracy of finding a quasar decreases (lower efficiency). The values for threshold, completeness and efficiency will of course depend on galactic latitude (Ross et al. 2011). BOSS year-one data targeted using the Likelihood method at 20 targets deg⁻² for the CORE sample.

Although we targeted a number of tiles for spectroscopy during the first year of data taking, observational success was varied. Due to a combination of poor observing conditions and equipment glitches, spectroscopic completeness (the fraction of total spectroscopic observations in a tiling region which yielded a high confidence spectroscopic identification upon visual inspection) was a strong function of the region in which a target was tiled. In this paper, we only test our method using observations in Stripe 82 regions with a spectroscopic completeness of $> 90\%$. In Fig. (2) we show the tiles used for testing.

To test the performance of our Likelihood method, we calculated probabilities using Eq. (3) on single-epoch data in regions of Stripe 82 with high spectroscopic completeness and compared that target list with the BOSS “truth table” (which includes targets from all targeting methods, quasars targeted using variability, and all previously known quasars). This is a fair test because targeting in this region was conducted using co-added photometry and thus we are not testing the Likelihood method on a region that was targeted with the same

photometry.

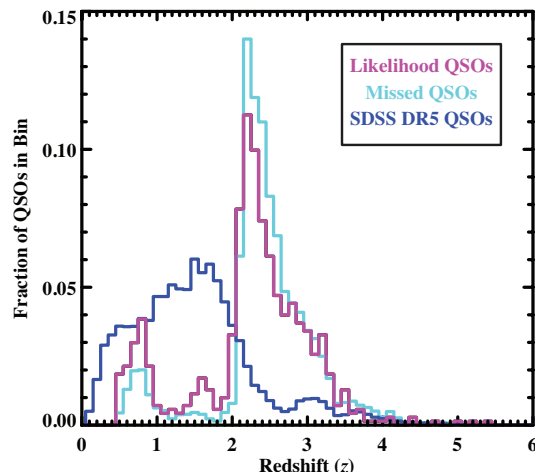


FIG. 5.— The redshift distributions of the Likelihood method recovered QSOs (*magenta*) and false-negative QSOs that were not targeted (missed) by the Likelihood method (*cyan*), compared with SDSS DR5 QSOs (*blue*).

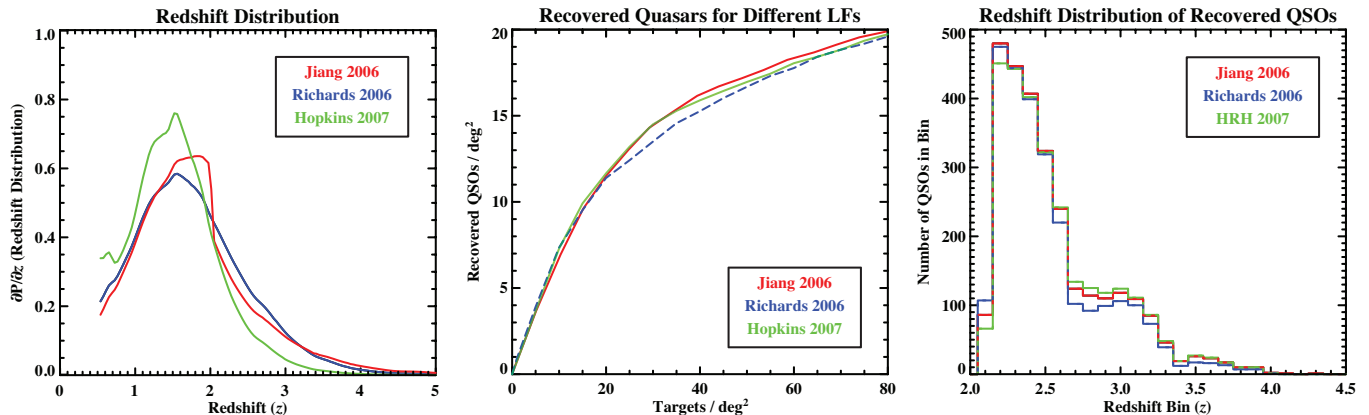


FIG. 6.— (*Left*) - Predicted redshift distribution for Jiang et al. (2006) (red), Richards et al. (2006) (blue) and Hopkins et al. (2007) (green) luminosity functions. (*Center*) - The number of BOSS quasars recovered as a function of targets deg^{-2} for the three luminosity functions (i.e. different priors). The performance of all three LFs is almost identical for target densities up to ~ 20 targets deg^{-2} , at which point the Richards model starts to perform slightly worse. (*Right*) - The redshift distributions of the recovered quasars for the three luminosity functions.

TABLE 2
LIKELIHOOD LUMINOSITY FUNCTION TESTING

Luminosity Function	Targets per deg^2	Likelihood \mathcal{P} Threshold	Total Targets	QSOs Recovered	QSOs Missed	Completeness (%)	Efficiency (%)
Jiang et al.	20	0.535	3878	2166	2401	47	56
	40	0.245	7757	3087	1657	65	40
Richards et al.	20	0.237	3978	2089	2466	46	54
	40	0.079	7757	2939	1808	62	37
Hopkins et al.	20	0.383	3878	2154	2401	47	56
	40	0.158	7737	3046	1676	64	39

NOTE. — Shows the completeness and efficiency as a function of dedicated target fibers (targets deg^{-2}) for three different luminosity functions. The three LFs tested are from Jiang et al. (2006), Richards et al. (2006), and Hopkins et al. (2007). These values are for $z > 2.2$ recovered/missed QSOs.

Likelihood probabilities were calculated for 592,847 objects; of those, the top 7,757 likelihoods were selected ($\mathcal{P} > 0.245$) for a target density of 40 objects per deg^2 . Fig. (3) shows the distribution of the likelihood probabilities for the recovered* and false-negative (missed) QSOs as well as for the false-positive stars (wrongly) targeted by the method. We found an efficiency (Recovered QSOs / Total Targets) of 40% and completeness (Likelihood Recovered QSOs / Total BOSS Recovered QSOs) of 65%. Fig. (4) shows *ugr* color-color plots of BOSS quasars recovered (magenta) and missed (cyan) by the Likelihood method as well as false positive contamination stars (red) that were targeted by the method.

There is of course the inevitable trade-off between efficiency and completeness. The more fibers given to quasar targets, the more QSOs are found (greater completeness), but the accuracy of targeting a quasar decreases (lower efficiency). This is shown in Table (1) where the rate of new targeted QSOs is shown to steadily decrease as a function of targets deg^{-2} .

By comparing the target objects to the catalog contours in Fig. (4), it is clear that the Likelihood method fails mostly in the region of overlap between the two catalogs. Fig. (5) shows the redshift distributions of the targeted and missed quasars and the limitation of SDSS

* We defined recovered/missed QSOs to be quasars in the desired BOSS redshift range ($z > 2.2$).

DR5 catalog at $z > 2$. Table (1) shows the detailed testing results.

4. TESTING, IMPROVEMENTS AND CONCLUSIONS

4.1. Luminosity Function Testing

We tested the performance of three different quasar luminosity functions (LFs) as inputs to the QSO Catalog. The LFs enter into the generation of the QSO Catalog by determining the density of quasars as a function of redshift and *i*-band magnitude. All the other details of the Monte Carlo remain the same as described in Section (2.2). The EE Catalog is not dependent on these LFs so this catalog stays the same for these tests. The three functions tested are from Jiang et al. (2006), Richards et al. (2006), and Hopkins et al. (2007). The inputs and results from this testing is shown in Fig. (6).

The quasar redshift distributions for these three luminosity functions are shown in the left panel of Fig. (6). The performance of the method did not change significantly for the three different LFs. Fig. (6) (*Center*) shows the number of quasars successfully recovered as a function of the number of dedicated QSO target fibers per deg^2 . Notice the shape of this function, the rate of newly recovered quasars drops off significantly beyond 40 targets deg^{-2} . The performance of all three LFs is essentially identical up to 20 targets deg^{-2} . The redshift distributions of the recovered quasars are slightly different as shown in Fig. (6) (*Right*), so using different LF

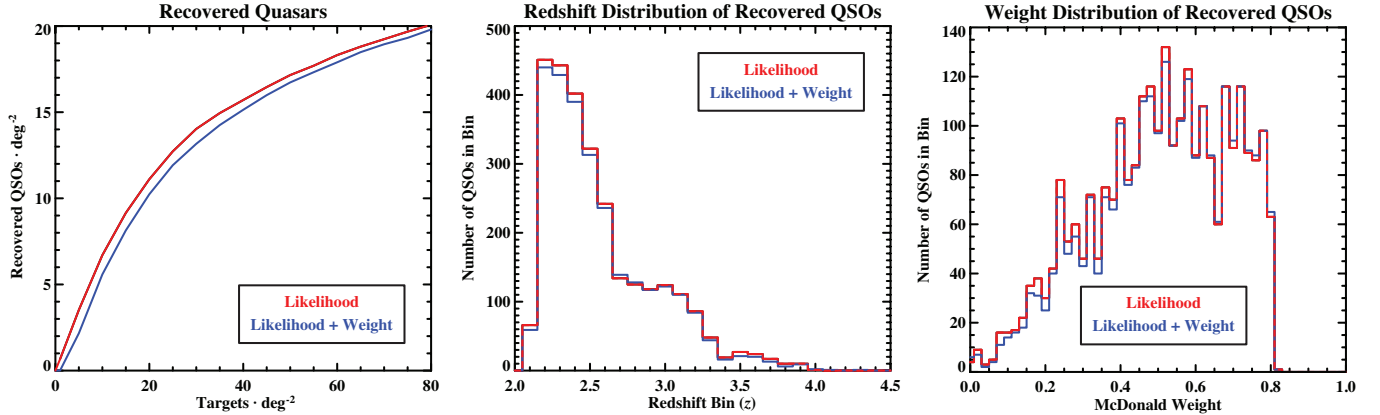


FIG. 7.— (Left) - The number of BOSS quasars recovered as a function of targets deg^{-2} for the Likelihood method with and without the weights. (Center) - The redshift distributions of the recovered quasars. (Right) - The weight distributions of the recovered quasars. Notice that using the Likelihood + weights recovers QSOs with a higher BAO value.

could be used to help tune the targeting redshifts.

Ultimately it was decided that Jiang et al. (2006) was the best luminosity function for our purposes because it was more efficient at recovering $z > 2.2$ QSOs than Richards et al. (2006) and Hopkins et al. (2007). More detailed values for the performance of these different luminosity functions can be seen in Table (2).

While we are not currently making a proper comparison of the redshift distributions of BOSS quasars and the redshift distributions of these luminosity functions, a future improvement would be to use a luminosity function generated from the redshift distribution of BOSS quasars, properly adjusted for the targeting selection function imprinted upon it, as the input to the Monte Carlo to see if this approach improves target selection. Another promising modification would be to add the photometry from BOSS quasars to the inputs to the Monte Carlo simulation.

4.2. Weighted Likelihoods

We also tested adjusting Eq. (1) to incorporate a weighting factor to optimize (in redshift-magnitude space) selection of objects with a high dark energy figure of merit (Albrecht et al. 2006). This weighting is done by simply adding a factor (w_i) inside the product based on the value of the QSO catalog quasar flux and redshift ($QSO_{if}(z)$):

$$\mathcal{L}_{QSO}(\Delta z) = \sum_i \prod_f \frac{w_i}{\sqrt{2\pi\sigma_f^2}} \exp\left(-\frac{[x_f - QSO_{if}(\Delta z)]^2}{2\sigma_f^2}\right) \quad (4)$$

We tested adjusting the Likelihood method in this manner with weights (w_i) calculated by Pat McDonald (private communication, see Fig. (8)). Here the weight is determined by the contribution of the quasar's Ly α F to the BAO signal; a higher weight yields a higher signal-to-noise BAO measurement.

The weight is a functional derivative of the overall BAO (distance-error)² with respect to the luminosity function. It can therefore be integrated over any achieved luminosity function (or summed over a set of quasars) to produce an estimate proportional to the BAO (distance-error)² that one would expect to achieve from that data set. There are two relevant factors affecting the value of a

quasar: the noise level in the spectrum, and the density of quasars at a given redshift. The low redshift cutoff comes primarily from the degradation in the signal-to-noise ratio at the blue end of the spectrograph, while the high- z tail-off comes from the diminishing density of quasars with which to perform a cross-correlation for Ly α F calculations.

While using these weights did recover QSOs with a higher on average BAO signal, as expected less total quasars were recovered using this scheme, see Fig. (7). Ultimately it was decided to optimize the number of recovered quasars rather than the BAO signal. Therefore this weighting scheme was not used in the final Likelihood targeting algorithm for BOSS. However, depending on the goals of the user, a weighting scheme could be useful for future targeting purposes.

The likelihood calculations can easily be extended to include other parameters besides the photometric fluxes in the exponentials in Eq. (1) and Eq. (2) if you had a large enough data set with a high signal-to-noise ratio to use for training. For example, variability information,

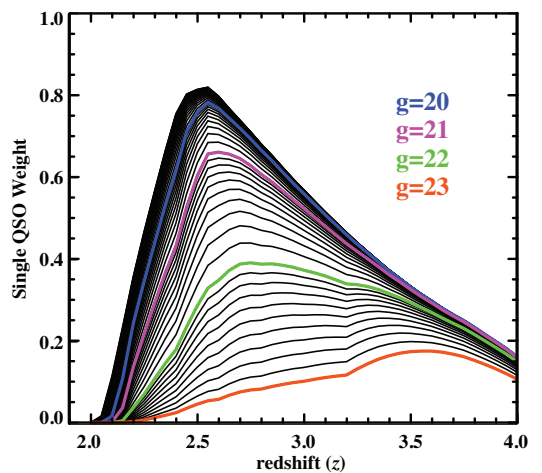


FIG. 8.— The McDonald Weight (or effectiveness as a dark energy BAO probe) of a QSO as a function of magnitude and redshift. The lines are at 0.1 magnitude intervals. Brighter quasars have a higher weight, and so do quasars centered around a $z \sim 2.5$.

sky position, UV and IR colors could each be incorporated if the user had such information in their data set.

4.3. Likelihood and XDQSO

The Likelihood method inspired a similar targeting approach, XDQSO (Bovy et al. 2011). The training sets used in XDQSO are almost identical to the QSO and EE Catalogs used in the Likelihood method. XDQSO uses an extreme-deconvolution fit to these catalogs, such that they are represented by a small set of Gaussian distributions instead of large set of discrete objects. Likelihood calculates probabilities as a straightforward sum over all objects, whereas XDQSO does a more algorithmically complicated fit. However, once the catalog Gaussians are determined, XDQSO probabilities are much faster to calculate than the likelihood probabilities. In the limit where the QSO and EE Catalogs are extremely large, and their photometric errors are very small, the two algorithms are essentially equivalent. However, for small, noisy data sets, Likelihood double counts the photometric errors and it also represents the continuous color-distribution of quasars as discrete delta functions in color-space which can produce noisier results. A study of the performance of the two methods shows that they are comparable in BOSS targeting efficiency, with XDQSO finding < 1 additional QSO deg^{-2} at a given threshold (Bovy et al. 2011).

4.4. Likelihood BOSS Targeting

After a commissioning period in September-November 2009, the QSO targeting fibers were dividing into a CORE and BONUS sample (Ross et al. 2011). The likelihood method, using the Jiang luminosity function was used for targeting the CORE sample (20 targets deg^{-2}) for the first year of BOSS data taking. The rest of the fibers (BONUS sample) were targeted by a combination of the output of the Likelihood, KDE and NN meth-

ods using a Neural Network. This approach allows us to combine both different methods and different photometric catalogs (SDSS, UKIDSS, GALEX) in the BONUS selection.

After the first year of data taking, in the targeting for the CORE sample the likelihood method was replaced with the XDQSO method (Bovy et al. 2011) and likelihood was then used in the BONUS sample as well as one of the inputs to the NN. We plan to release the likelihood probabilities from Eq. (3) in the project data releases of SDSS data.

Acknowledgments

Thank you to Pat McDonald, Jo Bovy, Erin Sheldon, and Michael Strauss for their contributions to this paper.

Funding for SDSS-III has been provided by the Alfred P. Sloan Foundation, the Participating Institutions, the National Science Foundation, and the U.S. Department of Energy. The SDSS-III web site is <http://www.sdss3.org/>.

SDSS-III is managed by the Astrophysical Research Consortium for the Participating Institutions of the SDSS-III Collaboration including the University of Arizona, the Brazilian Participation Group, Brookhaven National Laboratory, University of Cambridge, University of Florida, the French Participation Group, the German Participation Group, the Instituto de Astrofísica de Canarias, the Michigan State/Notre Dame/JINA Participation Group, Johns Hopkins University, Lawrence Berkeley National Laboratory, Max Planck Institute for Astrophysics, New Mexico State University, New York University, Ohio State University, Pennsylvania State University, University of Portsmouth, Princeton University, the Spanish Participation Group, University of Tokyo, University of Utah, Vanderbilt University, University of Virginia, University of Washington, and Yale University.

REFERENCES

- Abazajian, K. N. et al. 2009, *ApJS*, 182, 543
 Adelman-McCarthy, J. K. et al. 2008, *ApJS*, 175, 297
 Albrecht, A. et al. 2006, *ArXiv Astrophysics e-prints*
 Allen, J. T., Hewett, P. C., Maddox, N., Richards, G. T., & Belokurov, V. 2011, *MNRAS*, 410, 860
 Bahcall, J. N. & Goldsmith, S. 1971, *ApJ*, 170, 17
 Bovy, J. et al. 2011, *The Astrophysical Journal*, 729, 141
 Cattaneo, A. et al. 2009, *Nature*, 460, 213
 Croft, R. A. C., Weinberg, D. H., Katz, N., & Hernquist, L. 1998, *ApJ*, 495, 44
 Croft, R. A. C. et al. 2002, *ApJ*, 581, 20
 Croom, S. M., Richards, G. T., Shanks, T., Boyle, B. J., Strauss, M. A., Myers, A. D., Nichol, R. C., Pimbblet, K. A., Ross, N. P., Schneider, D. P., Sharp, R. G., & Wake, D. A. 2009, *MNRAS*, 399, 1755
 Croom, S. M. et al. 2004, *MNRAS*, 349, 1397
 —. 2005, *MNRAS*, 356, 415
 Eisenstein, D. J., et al. 2011, *ArXiv e-prints*
 Fan, X. 1999, *AJ*, 117, 2528
 Fan, X., Carilli, C. L., & Keating, B. 2006a, *ARA&A*, 44, 415
 Fan, X. et al. 2006b, *AJ*, 132, 117
 Fukugita, M., Ichikawa, T., Gunn, J. E., Doi, M., Shimasaku, K., & Schneider, D. P. 1996, *AJ*, 111, 1748
 Giannantonio, T. et al. 2006, *Phys. Rev. D*, 74, 063520
 Giannantonio, T. et al. 2008, *Phys. Rev. D*, 77, 123520
 Gibson, R. R. et al. 2009, *ApJ*, 692, 758
 Gunn, J. E. et al. 1998, *AJ*, 116, 3040
 —. 2006, *AJ*, 131, 2332
 Hennawi, J. F., Myers, A. D., Shen, Y., Strauss, M. A., Djorgovski, S. G., Fan, X., Glikman, E., Mahabal, A., Martin, C. L., Richards, G. T., Schneider, D. P., & Shankar, F. 2010a, *ApJ*, 719, 1672
 Hennawi, J. F. et al. 2006a, *The Astronomical Journal*, 131, 1
 —. 2006b, *The Astrophysical Journal*, 651, 61
 —. 2010b, *ApJ*, 719, 1672
 Hogg, D. W., Finkbeiner, D. P., Schlegel, D. J., & Gunn, J. E. 2001, *AJ*, 122, 2129
 Hopkins, P. F., Richards, G. T., & Hernquist, L. 2007, *The Astrophysical Journal*, 654, 731
 Ivezić, Ž. et al. 2004, *Astronomische Nachrichten*, 325, 583
 Jiang, L. et al. 2006, *AJ*, 131, 2788
 Lawrence, A. et al. 2007, *MNRAS*, 379, 1599
 Lupton, R., Gunn, J. E., Ivezić, Z., Knapp, G. R., & Kent, S. 2001, in *Astronomical Society of the Pacific Conference Series*, Vol. 238, *Astronomical Data Analysis Software and Systems X*, ed. F. R. Harnden Jr., F. A. Primini, & H. E. Payne, 269
 Lynds, R. 1971, *ApJ*, 164, L73+
 Martin, D. C. et al. 2005, *ApJ*, 619, L1
 Matthews, T. A. & Sandage, A. R. 1963, *ApJ*, 138, 30
 McDonald, P. 2003, *The Astrophysical Journal*, 585, 34
 McDonald, P. & Eisenstein, D. J. 2007, *Phys. Rev. D*, 76, 063009
 McDonald, P. et al. 2006, *ApJS*, 163, 80
 McQuinn, M. & White, M. 2011, *ArXiv e-prints*
 Meiksin, A. A. 2009, *Reviews of Modern Physics*, 81, 1405
 Myers, A. D., Brunner, R. J., Nichol, R. C., Richards, G. T., Schneider, D. P., & Bahcall, N. A. 2007a, *ApJ*, 658, 85

- Myers, A. D., Brunner, R. J., Richards, G. T., Nichol, R. C., Schneider, D. P., & Bahcall, N. A. 2007b, *ApJ*, 658, 99
- Myers, A. D. et al. 2006, *ApJ*, 638, 622
- Myers, A. D. et al. 2008, *The Astrophysical Journal*, 678, 635
- Padmanabhan, N. et al. 2008, *ApJ*, 674, 1217
- Palanque-Delabrouille, N. et al. 2010, *ArXiv e-prints*
- Peth, M. A., Ross, N. P., & Schneider, D. P. 2011, *AJ*, 141, 105
- Pier, J. R., Munn, J. A., Hindsley, R. B., Hennessy, G. S., Kent, S. M., Lupton, R. H., & Ivezić, Z. 2003, *AJ*, 125, 1559
- Prochaska, J. X. & Hennawi, J. F. 2009, *The Astrophysical Journal*, 690, 1558
- Rauch, M. 1998, *ARA&A*, 36, 267
- Richards, G. T. et al. 2002, *AJ*, 123, 2945
- . 2004, *The Astrophysical Journal Supplement Series*, 155, 257
- . 2006, *The Astronomical Journal*, 131, 2766
- . 2009, *ApJS*, 180, 67
- Ross, N. P. et al. 2009, *ApJ*, 697, 1634
- . 2011, *ArXiv e-prints*
- Sandage, A. 1965, *ApJ*, 141, 1560
- Schlegel, D., White, M., & Eisenstein, D. 2009, in *ArXiv Astrophysics e-prints*, Vol. 2010, *astro2010: The Astronomy and Astrophysics Decadal Survey*, 314–+
- Schlegel, D. J., Blanton, M., Eisenstein, D., Gillespie, B., Gunn, J., Harding, P., McDonald, P., Nichol, R., Padmanabhan, N., Percival, W., Richards, G., Rockosi, C., Roe, N., Ross, N., Schneider, D., Strauss, M., Weinberg, D., & White, M. 2007, in *Bulletin of the American Astronomical Society*, Vol. 38, *American Astronomical Society Meeting Abstracts*, 132.29–+
- Schlegel, D. J., Finkbeiner, D. P., & Davis, M. 1998, *The Astrophysical Journal*, 500, 525
- Schmidt, K. B., Marshall, P. J., Rix, H. f., Jester, S., Hennawi, J. F., & Dobler, G. 2010, *ApJ*, 714, 1194
- Schmidt, M. 1963, *Nature*, 197, 1040
- Schneider, D. P. et al. 2007, *AJ*, 134, 102
- . 2010, *AJ*, 139, 2360
- Scranton, R. et al. 2005, *The Astrophysical Journal*, 633, 589
- SDSS-III collaboration et al. 2011, *ArXiv e-prints*
- Shankar, F. 2009, *ArXiv e-prints*, 53, 57
- Shen, Y. 2009, *PhD thesis*, Princeton University
- Shen, Y. et al. 2007, *AJ*, 133, 2222
- . 2009, *ApJ*, 697, 1656
- . 2010, *The Astrophysical Journal*, 719, 1693
- Slosar, A. et al. 2011, *ApJ*, in prep.
- Smith, J. A. et al. 2002, *AJ*, 123, 2121
- Stoughton, C. et al. 2002, *AJ*, 123, 485
- Tucker, D. L. et al. 2006, *Astronomische Nachrichten*, 327, 821
- Weymann, R. J., Carswell, R. F., & Smith, M. G. 1981, *ARA&A*, 19, 41
- Weymann, R. J., Morris, S. L., Foltz, C. B., & Hewett, P. C. 1991, *ApJ*, 373, 23
- White, M. 2003, in *The Davis Meeting On Cosmic Inflation*
- Willott, C. J. et al. 2010, *AJ*, 139, 906
- Yèche, C. et al. 2009, *ArXiv e-prints*
- . 2010, *A&A*, 523, A14+
- York, D. G. et al. 2000, *AJ*, 120, 1579